Article

Laser-Polarization Effects on Coherent Vibronic Excitation of Molecules with Quasi-Degenerate Electronic States

Manabu Kanno,[†] Yukari Ono,[†] Hirohiko Kono,[†] and Yuichi Fujimura*[,†,‡]

[†]Department of Chemistry, Graduate School of Science, Tohoku University, Sendai 980-8578, Japan
[‡]Department of Applied Chemistry, Institute of Molecular Science and Center for Interdisciplinary Molecular Science, Chiao-Tung University, Hsin-Chu, 300 Taiwan

ABSTRACT: The laser-polarization effects on nonadiabatically coupled π-electron rotation (ring current) and molecular vibration have been theoretically analyzed for aromatic molecules with quasi-degenerate excited states irradiated by an ultrashort laser pulse of arbitrary polarization. We first derived general formulations of the coherent electronic wave packet and expectation value of electronic angular momentum within a frozen-nuclei model. The relative quantum phase of the superposed quasi-degenerate states, which determines the oscillating behavior of angular momentum, can be manipulated by the ellipticity and orientation of the incident laser. Nuclear wave packet simulations with a model molecule confirmed the controllability of π-electron rotation, although the angular momentum is gradually reduced by nonadiabatic couplings. The amplitude of molecular vibration depends prominently on the orientation of linear polarization vectors rather than the helicity of circular polarization. The characteristic feature in vibrational amplitudes is attributed to the interference in nonadiabatic transition governed by the relative quantum phase between nuclear wave packets. This offers a new strategy for laser control of molecular vibrations through the wave packet interference in nonadiabatic transition.
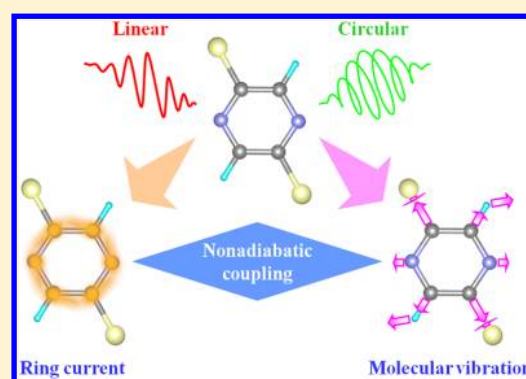
1. INTRODUCTION

Laser pulses with a duration ranging from attoseconds to several femtoseconds instantaneously change the electronic state of atomic and molecular systems. In recent years, control and observation of ultrafast dynamics in polyatomic molecules such as valence-electron motion and molecular vibration have been attempted by means of ultrashort laser pulses. For instance, from both experimental and theoretical aspects, time-resolved photoelectron angular distribution has been utilized to monitor the ultrafast dynamics through conical intersections, e.g., in the nonadiabatic transition in nitrogen dioxide NO_2,[1] in the photodissociation of carbon disulfide CS_2,[2] and in the internal conversions of aromatic hydrocarbons.[3−6] Each of the parameters that characterize a laser pulse plays a decisive role in the excitation of molecules; the light intensity of the pulse affects the number of molecules excited, the central frequency specifies the average energy absorbed by the molecules, and the pulse duration is related to the bandwidth of the incident laser. Among the parameters, laser polarization is attracting more and more attention as a key regulating factor of molecular motion. So far, intense polarized light pulses have been extensively employed for the alignment[7−12] and orientation[7,10,13−15] of molecules by manipulating their rotational states. The non-adiabatic alignment technique,[11,16] which achieves the field-free periodic alignment of linear[17−19] or nonlinear[20,21] molecules due to their rotational revival after pulse irradiation (from several tens of femtoseconds to picoseconds), has been used in

the first step of high harmonic generation[22−24] and molecular orbital (MO) tomography.[25−27]

Currently, it is an intriguing issue whether or not the vibronic dynamics of polyatomic molecules can be controlled by the polarization of shorter attosecond/several-femtosecond laser fields. For C_{60} fullerene, which is a large three-dimensional π-conjugated system, Hertel et al. has experimentally revealed that the patterns of multiphoton ionization and subsequent fragmentation caused by an intense femtosecond near-infrared laser depend significantly on optical ellipticity.[28] As for theoretical work, electronic and nuclear probability density currents or fluxes in molecules triggered by polarized femtosecond lasers have been actively investigated.[29−34] Among them, we refer to the quantum simulation by Barth et al. of laser-driven electron ring currents in Mg porphyrin, which is a planar two-dimensional π-conjugated system, i.e., an aromatic molecule.[29] The results of the simulation performed under a frozen-nuclei condition indicated that π electrons of the molecule can be rotated along its aromatic ring by applying a circularly polarized ultraviolet (UV) laser pulse. The circular motion of π electrons around the ring is associated with the angular momentum along the molecular axis perpendicular to

the ring plane. Mg porphyrin has a pair of doubly degenerate π-electronic excited states, which are the eigenstates of the electronic angular momentum with opposite signs, owing to its high molecular symmetry. On irradiation the spin angular momentum of a photon is transferred to π electrons to produce one of the eigenstates selectively, and therefore, the rotation direction of π electrons is predetermined by the helicity of circular polarization. Laser-induced electron dynamics in ring-shaped systems such as aromatic molecules have been reported by other authors as well;[35−38] in particular, Ulusoy and Nest have shown by optimal control simulations that the aromaticity of benzene can be switched off by exciting it to nonaromatic target states.[38]

In contrast to the work by Barth et al., we have demonstrated that transient rotation of π electrons in an ansa (planar-chiral) aromatic molecule can be induced along its aromatic ring by a linearly polarized UV laser pulse.[39] In this case, the origin of directional ring current is not photon helicity but the asymmetry of the molecule. Lowering the molecular symmetry breaks the degeneracy of relevant excited states. Ultrashort laser pulses can create a coherent superposition of optically allowed quasi-degenerate excited states. The relative quantum phase of the superposed quasi-degenerate states can be controlled by the polarization direction of the incident laser with respect to the spatial configuration of the molecule. Another controlling factor is the relative optical phase between different frequency components if a two-color laser is employed.[40] When the nonstationary electronic state is so adjusted, π electrons travel in an intended direction, clockwise or counterclockwise, around the ring. Moreover, as an extension to nonadiabatic vibrational dynamics coupled to the laser-driven π-electron rotation, we have also performed nuclear wave packet (WP) simulations including nonadiabatic interactions between quasi-degenerate excited states.[41] The amplitudes of vibronically coupled molecular vibrations in the quasi-degenerate electronic states dramatically vary depending on the initial rotation direction of π electrons, which is determined by the linear polarization direction. We have explained this in both intuitive[42] and analytical[43] ways as an interference effect between nuclear WPs caused by nonadiabatic transition. This finding suggests that the information on attosecond π-electron dynamics can be obtained by spectroscopic detection of femtosecond molecular vibrations.

In this paper, we further extend the series of our studies to investigate nonadiabatic dynamics of aromatic molecules with quasi-degenerate π-electronic excited states irradiated by an ultrashort laser pulse of arbitrary polarization. Theoretical and numerical analyses in molecular optical response are made on the basis of the time-dependent Schrödinger equation (TDSE) explicitly taking into account the polarization of an applied laser field. The comparison between the results for linear and circular polarizations exemplifies the laser-polarization effects on coherent vibronic motion. We thereby establish a general optical control scheme for nonadiabatic dynamics of aromatic molecules with quasi-degenerate excited states.

The remainder of this paper is organized as follows. In section 2, first, we describe the concept of electronic angular momentum for aromatic molecules in terms of MO theory so as to introduce approximate angular momentum eigenstates in a quasi-degenerate system. Next, the optical excitation process is theoretically analyzed within a frozen-nuclei model to clarify the laser-polarization dependence of the relative quantum phase of the superposed quasi-degenerate states. In section 3, we

present the numerical results of nuclear WP simulations for a model system with a six-membered ring excited by linearly and circularly polarized UV laser pulses. It is shown that noticeable polarization-dependent nonadiabatic effects are found in both electronic angular momentum and vibrational amplitudes. We also discuss the laser control of the interference between nuclear WPs of the quasi-degenerate states in nonadiabatic transition. Finally, section 4 concludes this paper.

2. THEORY

2.1. Molecular Symmetry and Angular Momentum Eigenstates.
First of all, let us begin with a description of angular momentum eigenstates of π electrons in an aromatic molecule of D_{Nh} symmetry. The z axis is taken to be the C_N axis. According to MO theory, complex MOs $\{|\pi_m\rangle\}$ of the molecule are given as linear combinations of atomic orbitals (LCAO-MOs) in the form[44]

$$|\pi_m\rangle = \frac{1}{N^{1/2}} \sum_{j=1}^{N} \exp\left(im\frac{2j\pi}{N}\right)|p_{zj}\rangle$$

$$= \frac{1}{N^{1/2}} \sum_{j=1}^{N} \exp(im\phi_j)|p_{zj}\rangle \tag{1}$$

where $\phi_j \equiv 2j\pi/N$ and $|p_{zj}\rangle$ denote the azimuthal angle and p_z orbital at the jth atom in the aromatic ring, respectively. When N is an odd (even) number, the integer m reads $m = -(N-1)/2, ..., 0, ... (N-1)/2$ ($-N/2 + 1, ..., 0, ..., N/2$). The energy levels of $\{|\pi_m\rangle\}$ are well-known as a Frost circle:[45] $|\pi_0\rangle$ is the lowest MO and, for the other values of m, $|\pi_m\rangle$ and $|\pi_{-m}\rangle$ are degenerate. For odd N, $|\pi_{\pm(N-1)/2}\rangle$ are the highest MOs; for even N, the nondegenerate $|\pi_{N/2}\rangle$ is the highest. When a molecular polygon is approximated with a complete cylindrical ring, the symmetry of the molecule becomes $D_{\infty h}$ and the z component of electronic angular momentum is quantized in units of $\hbar$. Note that the expansion coefficients $N^{-1/2} \exp(im\phi_j)$ in eq 1 have the same mathematical form as the eigenfunctions of the angular momentum operator $\hat{l}_z = -i\hbar\partial/\partial\phi$, $(2\pi)^{-1/2} \exp(im\phi)$, except for the normalization constant. Hence, the complex MO $|\pi_m\rangle$ can be regarded as an angular momentum eigenstate and its eigenvalue of $\hat{l}_z$ is $m\hbar$ for degenerate MOs or zero for nondegenerate ones.

Here, we define real MOs $|\pi_{mx}\rangle$ and $|\pi_{my}\rangle$ ($m > 0$) as linear combinations of the complex degenerate ones $|\pi_m\rangle$ and $|\pi_{-m}\rangle$:

$$|\pi_{mx}\rangle \equiv 2^{-1/2}(|\pi_{+m}\rangle + |\pi_{-m}\rangle) \tag{2a}$$

$$|\pi_{my}\rangle \equiv -2^{-1/2}i(|\pi_{+m}\rangle - |\pi_{-m}\rangle) \tag{2b}$$

The expansion coefficients for $|p_{zj}\rangle$ in $|\pi_{mx}\rangle$ and $|\pi_{my}\rangle$ are $(2/N)^{1/2} \cos m\phi_j$ and $(2/N)^{1/2} \sin m\phi_j$, respectively. From eqs 2a and 2b, one readily finds

$$|\pi_{\pm m}\rangle = 2^{-1/2}(|\pi_{mx}\rangle \pm i|\pi_{my}\rangle) \tag{3}$$

Recalling that complex AOs $|2p_{+1}\rangle$ and $|2p_{-1}\rangle$ are angular momentum eigenstates of an electron in a hydrogen atom, the relation in eq 3 is similar to that between the complex AOs and real ones $|2p_x\rangle$ and $|2p_y\rangle$ with the real azimuthal functions $\pi^{-1/2} \cos\phi$ and $\pi^{-1/2} \sin\phi$, respectively.

On the basis of the concept of angular momentum eigenstates, we next explain the mechanism of π-electron rotation in Mg porphyrin interacting with a circularly polarized laser pulse[29] as an example. Mg porphyrin belongs to the D_{4h}

point group and its highest occupied and lowest unoccupied MOs (HOMO and LUMO) are nondegenerate a_{1u} and doubly degenerate e_g orbitals, respectively.[46,47] The degenerate LUMOs are one-electron angular momentum eigenstates with $m = \pm 1$. As for multielectron states constructed from MOs, Mg porphyrin has doubly degenerate ^1E_u excited states whose major components are single excitations from nondegenerate MOs such as the HOMO to the LUMOs. The degenerate excited states are viewed as the eigenstates of the total angular momentum operator $\hat{L}_z$ of the multielectron system with the quantum number $M = \pm 1$. As in the case of MOs, the multielectron angular momentum eigenstates $|^1E_{u\pm}\rangle$ with $M = \pm 1$ can be expressed as linear combinations of real excited states $|^1E_{ux}\rangle$ and $|^1E_{uy}\rangle$:

$$|^1E_{u\pm}\rangle = 2^{-1/2}(|^1E_{ux}\rangle \pm i|^1E_{uy}\rangle) \tag{4}$$

When a circularly polarized laser pulse is applied to Mg porphyrin propagating along its C_4 axis, the spin angular momentum of a photon selects $|^1E_{u+}\rangle$ or $|^1E_{u-}\rangle$ and π electrons start to rotate clockwise or counterclockwise depending on the selected state. This is the origin of the unique correspondence between the rotation direction of π electrons and that of the polarization plane of a circularly polarized laser pulse. In this way, one immediately recognizes that a linearly polarized laser pulse, which has no spin angular momentum, cannot rotate π electrons in Mg porphyrin.

If the molecular symmetry is lowered, e.g., by introducing functional groups and/or replacing some carbon atoms in the aromatic ring with heteroatoms, no two-dimensional irreducible representation E is allowed to exist and, accordingly, relevant MOs or multielectron states are not degenerate. There exists no excited state that is an eigenstate of $\hat{L}_z$ in such a system. Then, how can π-electron rotation be triggered in an aromatic molecule with quasi-degenerate excited states by light? Ultrashort laser pulses can coherently prepare a linear combination of the optically allowed quasi-degenerate states. With the notations of the real wave functions $|L\rangle$ and $|H\rangle$ for the lower and higher of the quasi-degenerate excited states, respectively, the approximate angular momentum eigenstates can be defined as

$$| \pm \rangle \equiv 2^{-1/2}(|L\rangle \pm i|H\rangle) \tag{5}$$

where the matrix elements $\langle \pm|\hat{L}_z|\pm\rangle$ are close to $\pm\hbar$. We denote the angular frequency of $|L\rangle$ ($|H\rangle$) by ω_L (ω_H). Because of the nonzero energy gap between the quasi-degenerate states, $|+\rangle$ or $|-\rangle$ prepared by a laser pulse subsequently evolves in time as a coherent nonstationary state:

$$e^{-i\hat{H}_0 t/\hbar}| \pm \rangle = 2^{-1/2}(e^{-i\omega_L t}|L\rangle \pm ie^{-i\omega_H t}|H\rangle)$$
$$= e^{-i\omega_L t}2^{-1/2}(|L\rangle \pm ie^{-i2\Delta\omega t}|H\rangle) \tag{6}$$

where $\hat{H}_0$ is the field-free electronic Hamiltonian and $2\Delta\omega \equiv \omega_H - \omega_L$. The approximate angular momentum eigenstates can be transiently created within the period of the electronic-state change, $T \equiv \pi/\Delta\omega$. Selective generation of an approximate angular momentum eigenstate is expected to bring about transient rotation of π electrons along an aromatic ring. The strategy for generating predominantly either $|+\rangle$ or $|-\rangle$ by a laser field will be discussed in section 2.2.

2.2. Optical Excitation Process within a Frozen-Nuclei Model. We focus on the theoretical analysis of the optical excitation process in aromatic molecules with quasi-degenerate

excited states, in particular, on the effects of laser polarization. Here, nuclear degrees of freedom are all ignored.

2.2.1. V-Type Three-Level Model. The time-dependent electronic Hamiltonian of a molecule interacting with a classical laser field $\varepsilon(t)$ is expressed in the length gauge under the dipole approximation as

$$\hat{H}(t) = \hat{H}_0 - \hat{\boldsymbol{\mu}} \cdot \boldsymbol{\varepsilon}(t) \tag{7}$$

where $\hat{\boldsymbol{\mu}}$ is the electric dipole moment operator. The TDSE for an electronic WP is

$$i\hbar \frac{\partial}{\partial t}|\Psi(t)\rangle = \hat{H}(t)|\Psi(t)\rangle \tag{8}$$

with the initial condition $|\Psi(0)\rangle = |G\rangle$, where $|G\rangle$ is the electronic ground state. To analytically solve the TDSE 8, we adopt the so-called V-type three-level model.[48a] In this model, the state vector of the system, $|\Psi(t)\rangle$, is expanded in terms of the minimum set, i.e., the ground and quasi-degenerate excited states:

$$|\Psi(t)\rangle = c_G(t)|G\rangle + c_L(t)e^{-i\omega_L t}|L\rangle + c_H(t)e^{-i\omega_H t}|H\rangle \tag{9}$$

where the angular frequency of $|G\rangle$, ω_G, is set to be zero. The optically allowed quasi-degenerate states $|L\rangle$ and $|H\rangle$ are independently coupled to $|G\rangle$, that is, $\langle L|\hat{\boldsymbol{\mu}}|H\rangle = \langle H|\hat{\boldsymbol{\mu}}|L\rangle = 0$; the other off-diagonal matrix elements of $\hat{\boldsymbol{\mu}}$ are real. For simplicity, all the diagonal elements of $\hat{\boldsymbol{\mu}}$ are assumed to be zero, although this assumption is not necessary for our model analysis to be valid. When eq 9 is inserted into eq 8, the equation of motion for the expansion coefficient vector $\mathbf{C}(t) \equiv (c_G(t), c_L(t), c_H(t))^T$ is derived as

$$\frac{d\mathbf{C}(t)}{dt} = i \begin{pmatrix} 0 & g_L(t) & g_H(t) \\ g_L(t)^* & 0 & 0 \\ g_H(t)^* & 0 & 0 \end{pmatrix} \mathbf{C}(t) \tag{10}$$

where

$$g_n(t) \equiv \frac{\langle G|\hat{\boldsymbol{\mu}}|n\rangle \cdot \boldsymbol{\varepsilon}(t)}{\hbar} e^{-i\omega_n t} \qquad (n = L \text{ and } H) \tag{11}$$

and the initial condition is $\mathbf{C}(0) = (1, 0, 0)^T$. For notational convenience, we denote $\boldsymbol{\mu}_n \equiv \langle G|\hat{\boldsymbol{\mu}}|n\rangle = \langle n|\hat{\boldsymbol{\mu}}|G\rangle$. A set of three-dimensional Cartesian coordinates x, y, and z is introduced so that both $\boldsymbol{\mu}_L$ and $\boldsymbol{\mu}_H$ can be expanded in terms of the unit vectors $\mathbf{e}_x$ and $\mathbf{e}_y$ only (Figure 1a): $\boldsymbol{\mu}_n = \mu_{nx}\mathbf{e}_x + \mu_{ny}\mathbf{e}_y$ ($n = L$ and H).

The laser field is supposed to propagate in the z direction and thus $\boldsymbol{\varepsilon}(t)$ oscillates in the xy plane. Its mathematical form is given by

$$\boldsymbol{\varepsilon}(t) = \frac{\varepsilon_p}{2}f(t)[e^{-i(\omega t+\varphi)}\mathbf{e} + e^{i(\omega t+\varphi)}\mathbf{e}^*] \tag{12}$$

where ε_p is the peak field strength, ω is the central frequency, φ is the optical phase, and $\mathbf{e}$ is the complex polarization unit vector. The time-dependent envelope function $f(t)$ slowly varies between zero and unity for $0 \leq t \leq t_d$ with t_d being the pulse duration; otherwise, $f(t) = 0$. The central frequency ω is set to be resonant with the average energy of the quasi-degenerate states: $\omega = \omega_L + \Delta\omega = \omega_H - \Delta\omega$. The general expression of $\mathbf{e}$ for an arbitrary (elliptical) polarization is

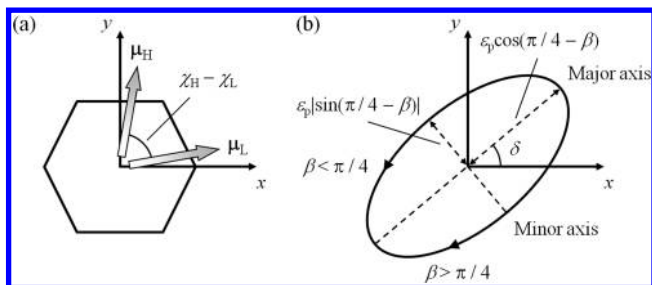$$\mathbf{e} = e^{-i\delta}(\cos\beta)\mathbf{e}_{+1} + e^{i\delta}(\sin\beta)\mathbf{e}_{-1} \tag{13}$$

Figure 1. (a) Spatial configurations of transition moments $\boldsymbol{\mu}_L$ and $\boldsymbol{\mu}_H$ and (b) orientation of the polarization ellipse. An aromatic molecule is represented by a hexagon. The x and y axes are chosen so that both $\boldsymbol{\mu}_L$ and $\boldsymbol{\mu}_H$ lie in the xy plane; in a degenerate system, the two axes can be parallel to the directions of the transition moments. $\chi_H - \chi_L$ denotes the angle between $\boldsymbol{\mu}_L$ and $\boldsymbol{\mu}_H$. The laser field propagates in the z direction and oscillates in the xy plane. The orientation angle of the major axis of the polarization ellipse with respect to the x axis is represented by δ. The minor-to-major axial ratio is $|\tan(\pi/4 - \beta)|$.

where $\mathbf{e}_{+1}$ and $\mathbf{e}_{-1}$ are the spherical unit vectors corresponding to positive and negative helicities (spins), respectively, defined as

$$\mathbf{e}_{\pm 1} \equiv 2^{-1/2}(\mathbf{e}_x \pm i\mathbf{e}_y) \tag{14}$$

Following the convention in optics, we refer to $\mathbf{e}_{+1}$ ($\mathbf{e}_{-1}$) as left (right) circular polarization. In eq 13, δ represents the orientation angle of the major axis of the polarization ellipse with respect to the x axis and β is called the ellipticity angle (Figure 1b). The value of β ranges from zero to $\pi/2$ and the minor-to-major axial ratio of the polarization ellipse is equal to $|\tan(\pi/4 - \beta)|$; specific examples are $\beta = 0$, $\pi/4$, and $\pi/2$ for left circular, linear, and right circular polarizations, respectively. Substituting eq 12 into eq 11 yields

$$g_L(t) = \frac{f(t)}{2}\{\Omega_L e^{-i[(2\omega - \Delta\omega)t + \varphi]} + \Omega_L^* e^{i(\Delta\omega t + \varphi)}\} \tag{15a}$$

$$g_H(t) = \frac{f(t)}{2}\{\Omega_H e^{-i[(2\omega + \Delta\omega)t + \varphi]} + \Omega_H^* e^{-i(\Delta\omega t - \varphi)}\} \tag{15b}$$

where $\Omega_n \equiv (\varepsilon_p/\hbar)\boldsymbol{\mu}_n \cdot \mathbf{e}$ ($n = $ L and H) are the complex Rabi frequencies. Here, we resort to the rotating-wave approximation (RWA),[48b] in which the contribution of the rapidly oscillating exponentials, i.e., the first terms in eqs 15a and 15b, to the time evolution of $\mathbf{C}(t)$ is averaged out and removed ($\omega \gg \Delta\omega$). Under the RWA, eq 10 is rewritten as

$$\frac{d\mathbf{C}(t)}{dt} = i\frac{f(t)}{2}$$
$$\begin{pmatrix} 0 & \Omega_L^* e^{i(\Delta\omega t + \varphi)} & \Omega_H^* e^{-i(\Delta\omega t - \varphi)} \\ \Omega_L e^{-i(\Delta\omega t + \varphi)} & 0 & 0 \\ \Omega_H e^{i(\Delta\omega t - \varphi)} & 0 & 0 \end{pmatrix} \mathbf{C}(t) \tag{16}$$

For the purpose of efficiently producing an approximate angular momentum eigenstate $|+\rangle$ or $|-\rangle$ defined in eq 5, the quasi-degenerate states $|L\rangle$ and $|H\rangle$ need to be populated equally. The laser field is therefore assumed to satisfy $|\Omega_L| = |\Omega_H|$ or, at least, $|\Omega_L| \simeq |\Omega_H|$. This leads to the orthogonality

$$(e^{i\theta}\boldsymbol{\mu}_L - \boldsymbol{\mu}_H) \cdot \mathbf{e} = 0 \tag{17}$$

where θ is an arbitrary phase between Ω_L and Ω_H, that is, $\theta \equiv \arg(\Omega_H/\Omega_L)$, and eq 17 requires

$$e^{i2\delta}\tan\beta = -\frac{(e^{i\theta}\boldsymbol{\mu}_L - \boldsymbol{\mu}_H) \cdot \mathbf{e}_{+1}}{(e^{i\theta}\boldsymbol{\mu}_L - \boldsymbol{\mu}_H) \cdot \mathbf{e}_{-1}} \tag{18}$$

Hence, the condition $|\Omega_L| = |\Omega_H|$ can be met with the ellipticity angle β and orientation angle δ determined by the absolute value and argument of the right-hand side of eq 18, respectively. To further simplify eq 16, we introduce the alternative pair of superposition states

$$|S_{\pm}\rangle \equiv \frac{1}{\bar{\Omega}}(\Omega_L|L\rangle \pm \Omega_H|H\rangle) = \frac{\Omega_L}{\bar{\Omega}}(|L\rangle \pm e^{i\theta}|H\rangle) \tag{19}$$

where $\bar{\Omega} \equiv (|\Omega_L|^2 + |\Omega_H|^2)^{1/2} = 2^{1/2}|\Omega_L| = 2^{1/2}|\Omega_H|$. They are normalized and orthogonal to each other because of the overlap $\langle S_+|S_-\rangle = (|\Omega_L|^2 - |\Omega_H|^2)/\bar{\Omega}^2 = 0$. Using these superposition states, the electronic WP can be expanded as

$$|\Psi(t)\rangle = c_G(t)|G\rangle + e^{-i(\omega t + \varphi)}[c_+(t)|S_+\rangle + c_-(t)|S_-\rangle] \tag{20}$$

where

$$c_{\pm}(t) \equiv \frac{1}{\bar{\Omega}}[\Omega_L^* e^{i(\Delta\omega t + \varphi)}c_L(t) \pm \Omega_H^* e^{-i(\Delta\omega t - \varphi)}c_H(t)] \tag{21}$$

Then, eq 16 can be converted to the equation of motion for the new coefficient vector $\mathbf{D}(t) \equiv (c_G(t), c_+(t), c_-(t))^T$:

$$\frac{d\mathbf{D}(t)}{dt} = \frac{i}{2}\begin{pmatrix} 0 & \bar{\Omega}f(t) & 0 \\ \bar{\Omega}f(t) & 0 & 2\Delta\omega \\ 0 & 2\Delta\omega & 0 \end{pmatrix}\mathbf{D}(t) \tag{22}$$

with the initial condition $\mathbf{D}(0) = (1, 0, 0)^T$.

2.2.2. Relative Quantum Phase between Degenerate Excited States. Before proceeding to the solution of eq 22 for a quasi-degenerate system, let us consider the degenerate case $\Delta\omega = 0$. In this case, eq 22 becomes extremely compact:

$$\frac{d\mathbf{D}(t)}{dt} = i\frac{\bar{\Omega}}{2}f(t)\begin{pmatrix} 0 & 1 & 0 \\ 1 & 0 & 0 \\ 0 & 0 & 0 \end{pmatrix}\mathbf{D}(t) \tag{23}$$

This clearly indicates that the system can be treated in practice as a two-level one consisting of $|G\rangle$ and $|S_+\rangle$. One can easily integrate eq 23 to obtain

$$\mathbf{D}(t) = \begin{pmatrix} \cos\left[\dfrac{\bar{\Omega}}{2}F(t)\right] \\ i\sin\left[\dfrac{\bar{\Omega}}{2}F(t)\right] \\ 0 \end{pmatrix} \tag{24}$$

where $F(t) \equiv \int_0^t du\, f(u)$. Within the RWA, complete population inversion from $|G\rangle$ to $|S_+\rangle$ can be achieved by the so-called π pulse,[48c] which fulfills $\bar{\Omega}F(t_d) = \pi$. When eq 24 is inserted into eq 20, the electronic WP can be written as

$$|\Psi(t)\rangle = \cos\left[\frac{\bar{\Omega}}{2}F(t)\right]|G\rangle$$
$$+ i\frac{\Omega_L}{\bar{\Omega}}\sin\left[\frac{\bar{\Omega}}{2}F(t)\right]e^{-i(\omega t+\varphi)}(|L\rangle + e^{i\theta}|H\rangle) \quad (25)$$

The relative quantum phase between the degenerate excited states $|L\rangle$ and $|H\rangle$ coincides with that between the Rabi frequencies Ω_L and Ω_H, i.e., θ, which is independent of time and controllable by the ellipticity angle β and orientation angle δ. This implies that a desired superposition of the degenerate states can be created by tuning the polarization of an incident light properly. The populations of the exact angular momentum eigenstates $|+\rangle$ and $|-\rangle$, $P_{\pm}(t) \equiv |\langle\pm|\Psi(t)\rangle|^2$, are derived as

$$P_{\pm}(t) = \frac{1}{2}\sin^2\left[\frac{\bar{\Omega}}{2}F(t)\right](1 \pm \sin\theta) \quad (26)$$

From these populations, the expectation value of angular momentum, $L_z(t) \equiv \langle\Psi(t)|\hat{L}_z|\Psi(t)\rangle$, is

$$L_z(t) = \hbar[P_+(t) - P_-(t)] = \hbar\sin^2\left[\frac{\bar{\Omega}}{2}F(t)\right]\sin\theta \quad (27)$$

The sign of $L_z(t)$, i.e., the rotation direction of π electrons, is subject to the relative quantum phase θ and remains unchanged throughout the time evolution: π electrons flow in a sole direction even after a laser pulse ceases at $t = t_d$.

Let us revert to eq 18, which links the relative quantum phase θ with the ellipticity angle β and orientation angle δ. In general, for aromatic molecules with degenerate states, $\boldsymbol{\mu}_L$ and $\boldsymbol{\mu}_H$ have the same magnitude and are perpendicular to each other, that is, $\|\boldsymbol{\mu}_L\| = \|\boldsymbol{\mu}_H\|$ and $\boldsymbol{\mu}_L\cdot\boldsymbol{\mu}_H = 0$. The x and y axes can thus be chosen to be parallel to $\boldsymbol{\mu}_L$ and $\boldsymbol{\mu}_H$, respectively, so that $\mu_{Lx} = \mu_{Hy} \neq 0$ and $\mu_{Ly} = \mu_{Hx} = 0$; in the case of Mg porphyrin, this holds when $|L\rangle = |^1E_{ux}\rangle$ and $|H\rangle = |^1E_{uy}\rangle$). Consequently, eq 18 is reduced to

$$e^{i2\delta}\tan\beta = -\frac{e^{i\theta}-i}{e^{i\theta}+i} = e^{i\pi/2}\tan\left[\frac{1}{2}\left(\frac{\pi}{2}-\theta\right)\right] \quad (28)$$

which involves neither transition electric dipole moments nor spherical unit vectors and is purely imaginary. Given a value of β, there exist two solutions of eq 28:

$$\delta = \pm\frac{\pi}{4} \quad \text{and} \quad \theta = \frac{\pi}{2} \mp 2\beta \quad (29)$$

The major axis of the polarization ellipse with $\delta = \pi/4$ bisects the angle between $\boldsymbol{\mu}_L$ and $\boldsymbol{\mu}_H$; that with $\delta = -\pi/4$ is perpendicular to it. In both cases, the value of $L_z(t_d)$ for the π-pulse excitation is $\hbar\sin\theta = \hbar\cos 2\beta$. In the case of circular polarization in which $\beta = 0$ or $\pi/2$, the value of δ is indeterminate from eq 28 or 29; in fact, it can be chosen arbitrarily as will be mentioned in the next paragraph.

We present illustrative examples and the case of linear polarization ($\beta = \pi/4$) is taken as the first one; eq 13 is then rewritten as

$$\mathbf{e} = (\cos\delta)\mathbf{e}_x + (\sin\delta)\mathbf{e}_y \quad (30)$$

and δ determines the polarization direction. The Rabi frequencies Ω_L and Ω_H are thus real-valued and their relative phase θ takes either zero or π ($e^{i\theta} = \pm 1$). Hereafter, the linear polarization vectors for $\theta = 0$ and π are denoted by $\mathbf{e}_{in}$ and $\mathbf{e}_{out}$, respectively. From eq 29, the values of δ for the two

polarization vectors are $\delta_{in} = \pi/4$ and $\delta_{out} = -\pi/4$. As in eq 25, a linearly polarized laser pulse with the polarization vector $\mathbf{e}_{in}$ ($\mathbf{e}_{out}$) produces an in-phase (out-of-phase) superposition $|L\rangle + |H\rangle$ ($|L\rangle - |H\rangle$), which is an equal mixture of the exact angular momentum eigenstates $|+\rangle$ and $|-\rangle$: $P_+(t) = P_-(t)$ and thus $L_z(t) = 0$ for all t. π-electron rotation cannot be induced in a degenerate system by a linearly polarized laser pulse. Next, for circular polarization, $\beta = 0$ ($\pi/2$) reads $\mathbf{e} = e^{-i\delta}\mathbf{e}_{+1}$ ($e^{i\delta}\mathbf{e}_{-1}$) and δ acts as an additional optical phase. From the definition of θ as an argument of Ω_H/Ω_L, we have $\theta = \pm(\chi_H - \chi_L)$ for $\mathbf{e}_{\pm 1}$, where $\chi_H - \chi_L$ is the angle between $\boldsymbol{\mu}_L$ and $\boldsymbol{\mu}_H$, that is, $\tan\chi_n = \mu_{ny}/\mu_{nx}$ (n = L and H); therefore, $\theta = \pm\pi/2$ ($e^{i\theta} = \pm i$) in a degenerate system. Meanwhile, δ can be set to any value because eq 25 shows that the optical phase does not affect the superposition of the degenerate states. The superposition states $|S_{\pm}\rangle$ are equivalent to the exact angular momentum eigenstates $|\pm\rangle$ ($|\mp\rangle$) for left (right) circular polarization, whereas the population is transferred only to $|S_+\rangle$ as in eq 24. π electrons of the molecule circulate along its ring in the direction inherent to the eigenstate generated.

The above consequences for linear and circular polarizations are consistent with the discussion on optically induced π-electron rotation in Mg porphyrin in section 2.1. The phase factor $e^{i\theta}$ yielded by elliptical polarization is neither real nor purely imaginary regardless of whether $\delta = \pm \pi/4$. As seen in eqs 26 and 27, the resultant behavior of π electrons is intermediate between those for linear and circular polarizations: The rotation direction of π electrons is subject to the more populated of $|+\rangle$ or $|-\rangle$, whereas the magnitude of $L_z(t_d)$ is less than $\hbar$ even under complete population inversion by the π pulse.

2.2.3. Relative Quantum Phase between Quasi-Degenerate Excited States. Now, we turn to the quasi-degenerate case $\Delta\omega \simeq 0$. Because it is impossible to integrate eq 22 with an arbitrary envelope function $f(t)$, we restrict $f(t)$ to a rectangular form: $f(t) = 1$ for $0 \leq t \leq t_d$ and otherwise zero. Then, eq 22 becomes solvable: During irradiation,

$$\frac{d\mathbf{D}(t)}{dt} = \frac{i}{2}\begin{pmatrix} 0 & \bar{\Omega} & 0 \\ \bar{\Omega} & 0 & 2\Delta\omega \\ 0 & 2\Delta\omega & 0 \end{pmatrix}\mathbf{D}(t) \quad (31)$$

of which the solution is

$$\mathbf{D}(t) = \begin{pmatrix} \left(\frac{\bar{\Omega}}{\Omega}\right)^2\cos\left(\frac{\Omega}{2}t\right) + \left(\frac{2\Delta\omega}{\Omega}\right)^2 \\ i\frac{\bar{\Omega}}{\Omega}\sin\left(\frac{\Omega}{2}t\right) \\ -\frac{\bar{\Omega}(2\Delta\omega)}{\Omega^2}\left[1 - \cos\left(\frac{\Omega}{2}t\right)\right] \end{pmatrix} \quad (32)$$

The generalized Rabi frequency $\Omega \equiv [\bar{\Omega}^2 + (2\Delta\omega)^2]^{1/2}$ is the root-mean-square of the Rabi frequencies and the detuning frequency $2\Delta\omega$. One can immediately confirm that eq 32 for $\Delta\omega = 0$ is identical to eq 24 for $f(t) = 1$. The ground state $|G\rangle$ can be fully emptied by imposing $2\Delta\omega \leq \bar{\Omega}$ and $\Omega F(t_d) = \Omega t_d$ $= 2\arccos[-(2\Delta\omega/\bar{\Omega})^2]$ on the rectangular-envelope pulse. The pulse area of this laser field (named the full-excitation pulse) is larger than that of the π pulse, $\Omega F(t_d) = \Omega t_d = \pi$. Finally, we acquire the coherent electronic WP in a quasi-degenerate system:

$$|\Psi(t)\rangle = \left[\left(\frac{\bar{\Omega}}{\Omega}\right)^2 \cos\left(\frac{\Omega}{2}t\right) + \left(\frac{2\Delta\omega}{\Omega}\right)^2\right]|G\rangle$$
$$+ \ i\frac{\Omega_L}{\Omega}\alpha(t)e^{-i(\omega t+\varphi)}\{|L\rangle + e^{i[\theta-\theta(t)]}|H\rangle\} \qquad (33)$$

where

$$\alpha(t) \equiv \sin\left(\frac{\Omega}{2}t\right) + i\frac{2\Delta\omega}{\Omega}\left[1 - \cos\left(\frac{\Omega}{2}t\right)\right]$$
$$= 2\sin\left(\frac{\Omega}{4}t\right)\left[\cos\left(\frac{\Omega}{4}t\right) + i\frac{2\Delta\omega}{\Omega}\sin\left(\frac{\Omega}{4}t\right)\right]$$
$$= 2\sin\left(\frac{\Omega}{4}t\right)\bar{\alpha}(t) \qquad (34)$$

and $\vartheta(t) \equiv 2\arg\bar{\alpha}(t)$. The relative quantum phase between the quasi-degenerate excited states $|L\rangle$ and $|H\rangle$ is given by $\theta - \vartheta(t)$ and its temporal behavior is the main point of this model analysis. Using $\alpha(t)$ in eq 34, the populations $P_\pm(t)$ are expressed as

$$P_\pm(t) = \frac{1}{2}\left[\frac{\bar{\Omega}}{\Omega}|\alpha(t)|\right]^2\{1 \pm \sin[\theta - \theta(t)]\} \qquad (35)$$

and the angular-momentum expectation value $L_z(t)$ is

$$L_z(t) = L[P_+(t) - P_-(t)] = L\left[\frac{\bar{\Omega}}{\Omega}|\alpha(t)|\right]^2\sin[\theta - \theta(t)] \qquad (36)$$

where $\langle\pm|\hat{L}_z|\pm\rangle \equiv \pm L$ ($L > 0$). In distinction from eq 27, the rotation direction of π electrons can be reversed during irradiation owing to the presence of the time-dependent phase $\vartheta(t)$ in eq 36.

For aromatic molecules with quasi-degenerate states, eqs 28 and 29 do not strictly hold because in general lowering the molecular symmetry leads to $\|\boldsymbol{\mu}_L\| \neq \|\boldsymbol{\mu}_H\|$ and $\boldsymbol{\mu}_L \cdot \boldsymbol{\mu}_H \neq 0$. In this case, the linear polarization vectors $\mathbf{e}_{in}$ ($\theta = 0$) and $\mathbf{e}_{out}$ ($\theta = \pi$) can be derived by substituting eq 30 into eq 17:

$$\delta_{in,out} = \arctan\left(-\frac{\mu_{Lx} \mp \mu_{Hx}}{\mu_{Ly} \mp \mu_{Hy}}\right) \qquad (37)$$

It is straightforward to find a pair of β and δ for the other values of θ from eq 18 with the transition moments specified. Circular polarizations do not exactly satisfy eq 18, i.e., the condition $|\Omega_L| = |\Omega_H|$ unless the magnitudes of $\boldsymbol{\mu}_L$ and $\boldsymbol{\mu}_H$ happen to be equal ($\|\boldsymbol{\mu}_L\| = \|\boldsymbol{\mu}_H\|$). On the assumption that the energy gap between $|L\rangle$ and $|H\rangle$ is small ($\Delta\omega \simeq 0$), the relationship between β, δ, and θ should be close to that in the degenerate case; for example, $\mathbf{e}_{in}$ and $\mathbf{e}_{out}$ whose polarization directions are defined by eq 37 should be almost perpendicular to each other, and we approximately have $\pm i\Omega_L \simeq \Omega_H$ ($\theta \simeq \pm\pi/2$) for $\mathbf{e}_{\pm1}$.

The time-dependent part of the relative quantum phase, i.e., $\vartheta(t)$ follows

$$\tan\left[\frac{\theta(t)}{2}\right] = \frac{2\Delta\omega}{\Omega}\tan\left(\frac{\Omega}{4}t\right) \qquad (38)$$

from its definition. Hence, $\vartheta(t)$ evolves as $0 \to \pi/2 \to \pi \to 3\pi/2 \to 2\pi \to \ldots$ with the progression of time, $0 \to T_R - \gamma \to T_R \to T_R + \gamma \to 2T_R \to \ldots$, where $T_R \equiv 2\pi/\Omega$ is the period of the (generalized) Rabi oscillations and $\gamma \equiv 4\arctan(2\Delta\omega/\Omega)/\Omega$.

Because $2\Delta\omega \leq \Omega$, T_R is not larger than the period T of the field-free electronic-state change and $\gamma \leq T_R/2$. The relative quantum phase grows from its initial value θ in the negative direction by $\vartheta(t)$; if the full-excitation pulse is employed, $\vartheta(t_d) \leq \pi$ from the inequality $T_R/2 \leq 2\arccos[-(2\Delta\omega/\bar{\Omega})^2]/\Omega \leq T_R$. The populations $P_\pm(t)$ and the expectation value $L_z(t)$ vary in time according to the relative quantum phase $\theta - \vartheta(t)$ as shown in eqs 35 and 36, respectively.

After the laser pulse is turned off ($t > t_d$), the electronic WP propagates freely. In a fashion similar to that in eq 6, the relative quantum phase in the free propagation is $\theta - \vartheta(t_d) - 2\Delta\omega(t - t_d)$ and thereby the coherent superposition of the quasi-degenerate states oscillates with the period T. Eventually, the populations $P_\pm(t)$ and the expectation value $L_z(t)$ are also the oscillating functions of t in the form

$$P_\pm(t) = \frac{1}{2}\left[\frac{\bar{\Omega}}{\Omega}|\alpha(t_d)|\right]^2 \times$$
$$\{1 \pm \sin[\theta - \theta(t_d) - 2\Delta\omega(t - t_d)]\} \qquad (39)$$

and

$$L_z(t) = L\left[\frac{\bar{\Omega}}{\Omega}|\alpha(t_d)|\right]^2\sin[\theta - \theta(t_d) - 2\Delta\omega(t - t_d)] \qquad (40)$$

respectively. The approximate angular momentum eigenstates $|+\rangle$ and $|-\rangle$ are alternately generated as predicted in section 2.1, and therefore, the rotation direction of π electrons switches between clockwise and counterclockwise. This is a notable difference from the degenerate case, in which the rotation direction is fixed and the angular-momentum expectation value $L_z(t)$ is constant after the applied pulse fully decays.

We have formulated the coherent electronic WP $|\Psi(t)\rangle$ and the angular-momentum expectation value $L_z(t)$ of the quasi-degenerate system irradiated by a laser pulse of arbitrary polarization. It should be emphasized that, despite the subsequent oscillating behavior, the initial relative phase of the superposed quasi-degenerate states or the initial rotation direction of π electrons depends on θ, which can be manipulated by the ellipticity angle β and orientation angle δ of the incident laser. Generation of polarization-shaped femtosecond UV laser pulses has become experimentally realizable.[49,50] In section 3, comparison will be made between this frozen-nuclei model in a rectangular-envelope case and nuclear WP simulations for pulse excitation with smooth rise and decay.

2.3. Propagation of Nuclear Wave Packets including Nonadiabatic Couplings.

We describe the method of real-time nuclear WP propagation for nonadiabatically coupled vibronic dynamics. The initial nuclear WP is set to be the vibrational ground-state wave function of $|G\rangle$ and the system is then electronically excited by a laser pulse $\boldsymbol{\varepsilon}(t)$ of the form in eq 12. To include the effects of nonadiabatic couplings on the WP propagation, we take advantage of the diabatic representation. Rigorous construction of the adiabatic–diabatic unitary transformation matrix requires the nonadiabatic (derivative) coupling matrix,[51,52] which is usually difficult to compute. Instead, we utilize the quasi-diabatization scheme proposed by Simah et al.[53] that is based on an analysis of configuration interaction vectors; it has been implemented by the original authors in the quantum chemistry program MOLPRO.[54] The state vector of the system is expanded in terms of the three

diabatic states $\{|n^D\rangle\}$, each of which is a linear combination of the adiabatic states $|G\rangle$, $|L\rangle$, and $|H\rangle$. The time evolution of the expansion coefficients for $|n^D\rangle$, $\psi_n^D(\mathbf{Q},t)$, where $\mathbf{Q}$ is the mass-weighted nuclear position or vibrational mode vector, can be obtained from the following equations of motion:[55]

$$i\hbar \frac{\partial}{\partial t}\psi_n^D(\mathbf{Q},t) = -\frac{\hbar^2}{2}\nabla^2 \psi_n^D(\mathbf{Q},t)$$
$$+ \sum_{n'}[V_{nn'}^D(\mathbf{Q}) - \boldsymbol{\mu}_{nn'}^D(\mathbf{Q})\cdot\boldsymbol{\varepsilon}(t)]\psi_{n'}^D(\mathbf{Q},t)$$

$$(41)$$

where ∇^2 is the Laplacian with respect to $\mathbf{Q}$. $V_{nn'}^D(\mathbf{Q})$ are the diabatic potentials ($n = n'$) and couplings ($n \neq n'$) and $\boldsymbol{\mu}_{nn'}^D(\mathbf{Q})$ are the transition moments between the two diabatic states. The coupled equations can be integrated numerically with the split-operator method for a multisurface Hamiltonian.[56] The resultant diabatic WPs $\psi_n^D(\mathbf{Q},t)$ are converted to adiabatic WPs $\psi_n(\mathbf{Q},t)$.

3. RESULTS AND DISCUSSION

3.1. Model System. In this section, we present the numerical results of nuclear WP simulations for an aromatic molecule with a six-membered ring, 2,5-dichloropyrazine (DCP), which was also used as a model system in our previous studies.[41−43] The chemical formula of DCP is illustrated in Figure 2a. The molecule is assumed to be preoriented, e.g., by the nonadiabatic optical alignment technique.[11,16]
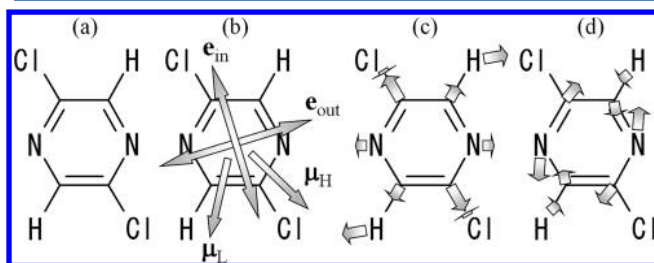

Figure 2. (a) Chemical formula of DCP. (b) Directions of transition moments $\boldsymbol{\mu}_L$ and $\boldsymbol{\mu}_H$ at the ground-state optimized geometry of DCP as well as those of linear polarization vectors $\mathbf{e}_{in}$ and $\mathbf{e}_{out}$ whose orientation angles are defined by eq 37. The magnitudes of $\boldsymbol{\mu}_L$ and $\boldsymbol{\mu}_H$ are $1.66ea_0$ and $1.58ea_0$, respectively, and the angle between them is $\chi_H - \chi_L = 0.35\pi$. The normal coordinates of the (c) breathing and (d) distortion modes are represented by thick arrows.

We performed all ab initio electronic structure computations for DCP with the 6-31G* Gaussian basis set[57] by using MOLPRO. Geometry optimization for the ground state was carried out at the level of the second-order Møller−Plesset perturbation theory (MP2)[57] and the optimized geometry was of C_{2h} symmetry. Then, to evaluate the excited-state properties at this geometry, the single-point ground- and excited-state calculation was executed at the state-averaged complete-active-space self-consistent field (CASSCF)[57] level of theory with ten active electrons and eight active (four a_u and four b_g) orbitals. At the optimized geometry in the ground state $|G\rangle = |1^1A_g\rangle$, DCP has a pair of optically allowed quasi-degenerate excited states, $|L\rangle = |3^1B_u\rangle$ and $|H\rangle = |4^1B_u\rangle$, with the energy gap $2\hbar\Delta\omega = 0.44$ eV (Table 1). The directions of the transition electric dipole moments between the ground and two excited states, $\boldsymbol{\mu}_L$ and $\boldsymbol{\mu}_H$, at this geometry are depicted in Figure 2b. The magnitudes of $\boldsymbol{\mu}_L$ and $\boldsymbol{\mu}_H$ are $1.66ea_0$ and $1.58ea_0$, respectively,

Table 1. Properties of Optically Allowed π-Electronic Excited States of DCP[a]

excited state	transition energy (eV)	oscillator strength
$|4^1B_u\rangle$	9.84	1.81
$|3^1B_u\rangle$	9.40	1.90
$|2^1B_u\rangle$	8.04	1.31
$|1^1B_u\rangle$	4.78	1.73×10^{-1}

[a]The excited states whose transition energies from $|G\rangle = |1^1A_g\rangle$ are less than 10.0 eV are listed. The ab initio geometry optimization for $|G\rangle$ and succeeding single-point calculation were carried out at the MP2/6-31G* and CASSCF(10,8)/6-31G* levels of theory, respectively.

and the angle between them is $\chi_H - \chi_L = 0.35\pi$. The approximate angular momentum eigenstates $|+\rangle$ and $|-\rangle$ in DCP are superpositions of $|L\rangle$ and $|H\rangle$ as in eq 5, where $\langle\pm|\hat{L}_z|\pm\rangle = \pm 0.98\hbar$. π electrons with positive (negative) angular momentum travel counterclockwise (clockwise) around the ring in Figure 2a.

The effective vibrational degrees of freedom for nuclear WP simulations were chosen by performing geometry optimizations for $|L\rangle$ and $|H\rangle$ at the CASSCF(10,8) level of theory. The optimized geometries of both $|L\rangle$ and $|H\rangle$ also belong to the C_{2h} point group. Hence, the displacements from the optimized geometry of $|G\rangle$ to that of $|L\rangle$ and $|H\rangle$ are totally symmetric. Furthermore, vibrational modes that couple two ^1B_u states are totally symmetric A_g modes as well. For these reasons, we consider two types of A_g normal modes with large potential displacements and nonadiabatic coupling matrix element, namely, breathing and distortion modes (Figure 2c,d) whose ground-state harmonic wave numbers are 1160 and 1570 cm^{-1}, respectively. Nonadiabatic couplings between the ground and two excited states were neglected because there is no potential crossing between them near the Franck−Condon region. The two-dimensional adiabatic potential energy surfaces (PESs) of $|L\rangle$ and $|H\rangle$ with respect to the normal coordinates $\mathbf{Q}$ of the breathing and distortion modes were calculated at the CASSCF(10,8) level of theory (Figure 3). There exists an
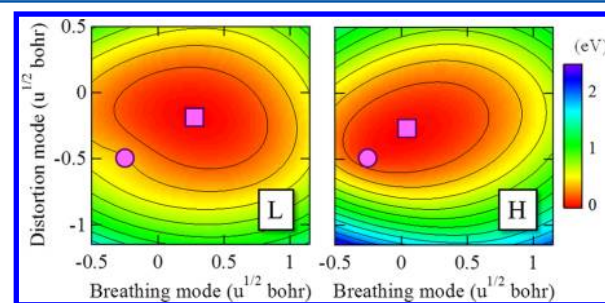

Figure 3. Two-dimensional adiabatic PESs of $|L\rangle$ and $|H\rangle$ with respect to the breathing and distortion modes of DCP. The origin of the PESs is the optimized geometry of $|G\rangle$. The minimum of each PES and the avoided crossing between them are designated by a square and circle, respectively.

avoided crossing (not a conical intersection) between the PESs, although whether it is an avoided crossing or a conical intersection does not influence the discussion below. The energy gap at the crossing point is about 190 cm^{-1}. We confirmed by a calculation at the level of the second-order CAS perturbation theory (CASPT2)[57] that the avoided crossing

remains unchanged when dynamical electron correlation is taken into account, whereas the PESs are lowered by ~3 eV.

The split-operator integration of eq 41 was executed with the aid of the fast Fourier transform algorithm. For each of the two modes, the domain $[-1.60 \, \mathrm{u}^{1/2}a_0, \, 1.55 \, \mathrm{u}^{1/2}a_0]$ was divided into 64 grid points at intervals of $0.05 \, \mathrm{u}^{1/2}a_0$ so as to represent nuclear WPs. The time step for the WP propagation was 2.4 as.

3.2. Nonadiabatic Transition between Quasi-Degenerate Excited States.

To elucidate the effects of laser polarization on nonadiabatically coupled π-electron rotation and molecular vibration, we compare the results of nuclear WP simulations for linear ($\beta = \pi/4$) and circular ($\beta = 0$ and $\pi/2$) polarizations. The orientation angles δ of the linear polarization vectors $\mathbf{e}_{\mathrm{in}}$ and $\mathbf{e}_{\mathrm{out}}$ were evaluated from eq 37 with the transition moments $\boldsymbol{\mu}_{\mathrm{L}}$ and $\boldsymbol{\mu}_{\mathrm{H}}$ at the optimized geometry of |G⟩ (Figure 2b). Note that an ultrashort laser pulse $\boldsymbol{\varepsilon}(t)$ vanishes before the WPs created on the two adiabatic PESs start to propagate, and accordingly, the coordinate dependence of $\boldsymbol{\mu}_{\mathrm{L}}(\mathbf{Q})$ and $\boldsymbol{\mu}_{\mathrm{H}}(\mathbf{Q})$ is important only in the Franck–Condon region, in which they are almost constant. For circular polarizations ($\mathbf{e}_{+1}$ and $\mathbf{e}_{-1}$), we set $\delta = 0$. The excitations by a laser pulse $\boldsymbol{\varepsilon}(t)$ with the four different polarization vectors are termed $\mathbf{e}_{\mathrm{in}}$, $\mathbf{e}_{\mathrm{out}}$, $\mathbf{e}_{+1}$, and $\mathbf{e}_{-1}$ excitations. Instead of the rectangular function adopted in the model analysis in section 2.2, we here assumed a $\sin^2$ envelope: $f(t) = \sin^2(\pi t/t_{\mathrm{d}})$ for $0 \leq t \leq t_{\mathrm{d}}$ and otherwise zero. The common laser parameters for the four types of excitations were $t_{\mathrm{d}} = 7.26$ fs, $\omega = 9.62$ eV/$\hbar$ (corresponding to the wavelength of 129 nm), and $\varphi = 0$. The peak field strength ε_{p} was determined in analogy to the full-excitation pulse in the rectangular-envelope case: $\Omega F(t_{\mathrm{d}}) = \Omega t_{\mathrm{d}}/2 = 2 \arccos[-(2\Delta\omega/\bar{\Omega})^2]$ with $2\Delta\omega \leq \bar{\Omega}$. The Rabi frequencies to meet this requirement for $t_{\mathrm{d}} = 7.26$ fs were $\bar{\Omega} = 0.62$ eV/$\hbar$ and $\Omega = 0.76$ eV/$\hbar$. The values of ε_{p} so determined for $\mathbf{e}_{\mathrm{in}}$, $\mathbf{e}_{\mathrm{out}}$, $\mathbf{e}_{+1}$, and $\mathbf{e}_{-1}$ excitations were 5.99, 9.80, 7.22, and 7.22 GV m^{-1}, respectively. Such high-intensity UV lights may induce two-photon excitations to higher excited states or ionizations but our previous studies[39,42] demonstrated that the contribution of these additional processes is not large. The use of weaker laser pulses does not affect the conclusions of this paper, although less population is transferred to the quasi-degenerate excited states. The results obtained for linear polarizations are very close to those reported in ref 41 for the π pulses whose peak field strengths are slightly lower with the smaller pulse area $\Omega F(t_{\mathrm{d}}) = \Omega t_{\mathrm{d}}/2 = \pi$. Because for DCP we have $\|\boldsymbol{\mu}_{\mathrm{L}}\| \simeq \|\boldsymbol{\mu}_{\mathrm{H}}\|$ in the vicinity of the optimized geometry of |G⟩, the condition $|\Omega_{\mathrm{L}}| \simeq |\Omega_{\mathrm{H}}|$ approximately holds for circular polarizations.

Figure 4 shows the temporal change in the populations of the quasi-degenerate states |L⟩ and |H⟩ for the four types of excitations. The populations on the two adiabatic PESs are defined as $P_n(t) \equiv \int d\mathbf{Q} \, |\psi_n(\mathbf{Q},t)|^2$ ($n = $ L and H). In all the four cases, it takes a few femtoseconds after a laser pulse $\boldsymbol{\varepsilon}(t)$ is turned on for $P_{\mathrm{L}}(t)$ and $P_{\mathrm{H}}(t)$ to increase because of the relatively slow rise of the $\sin^2$ envelope, whereas |L⟩ and |H⟩ begin to be populated within 1 fs by a rectangular-envelope pulse with the same peak field strength ε_{p}. A significant amount of the population is transferred to the quasi-degenerate states and divided almost equally between them at $t < 4$ fs. When the laser pulse ceases at $t = t_{\mathrm{d}} = 7.26$ fs, the total population in the quasi-degenerate states, $P_{\mathrm{L}}(t_{\mathrm{d}}) + P_{\mathrm{H}}(t_{\mathrm{d}})$, reaches 0.84, 0.93, 0.89, and 0.91 for $\mathbf{e}_{\mathrm{in}}$, $\mathbf{e}_{\mathrm{out}}$, $\mathbf{e}_{+1}$, and $\mathbf{e}_{-1}$ excitations, respectively. However, the subsequent behaviors of $P_{\mathrm{L}}(t)$ and $P_{\mathrm{H}}(t)$ are quite different between the four types of excitations. For $\mathbf{e}_{\mathrm{in}}$ excitation

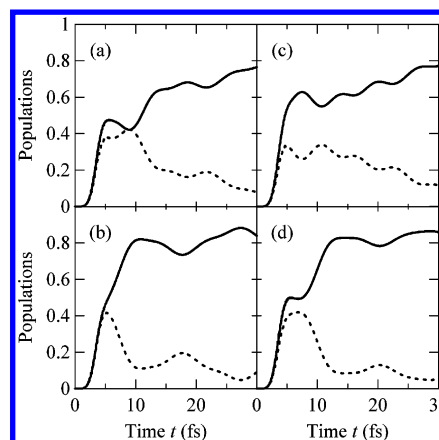**Figure 4.** Temporal behavior in the populations of the quasi-degenerate excited states for (a) $\mathbf{e}_{\mathrm{in}}$, (b) $\mathbf{e}_{\mathrm{out}}$, (c) $\mathbf{e}_{+1}$, and (d) $\mathbf{e}_{-1}$ excitations. In each panel, the solid line denotes the population of |L⟩; the dotted line denotes that of |H⟩. The laser pulses fully decay at $t = 7.26$ fs.

(Figure 4a), a small fraction of the population shifts from |L⟩ to |H⟩ by $t \sim 10$ fs and then a downward population transfer takes place around $t \sim 10$–14 fs by nonadiabatic transition. In the case of $\mathbf{e}_{\mathrm{out}}$ (Figure 4b), a considerable amount of the population is transferred from |H⟩ to |L⟩ and consequently $P_{\mathrm{L}}(t)$ is more than 7 times larger than $P_{\mathrm{H}}(t)$ at $t \sim 10$ fs. Afterward, the direction of population transfer is reversed periodically with the rather small portion of the population transferred. In contrast, the nonadiabatic transition for $\mathbf{e}_{+1}$ excitation persists much longer (Figure 4c): A part of the population is continuously exchanged between the quasi-degenerate states and thus electronic relaxation is completed after $t = 30$ fs. In the remaining case, i.e., $\mathbf{e}_{-1}$ excitation (Figure 4d), the behaviors of $P_{\mathrm{L}}(t)$ and $P_{\mathrm{H}}(t)$ are more or less intermediate between those for $\mathbf{e}_{\mathrm{in}}$ and $\mathbf{e}_{\mathrm{out}}$ excitations: A substantial population transfer from |H⟩ to |L⟩ is observed around $t \sim 8$–13 fs. These distinct patterns in the evolutions of $P_{\mathrm{L}}(t)$ and $P_{\mathrm{H}}(t)$ indicate that the polarization of the applied laser exerts a profound influence on the nonadiabatic transition between the quasi-degenerate states, which occurs mainly after irradiation.

3.3. Laser-Polarization Effects on Nonadiabatically Coupled Vibronic Dynamics.

The expectation value of electronic angular momentum $L_z(t)$ for the four types of excitations are plotted as a function of time in Figure 5. In the course of the interaction with the laser pulse $\boldsymbol{\varepsilon}(t)$, the timing of the initial increase in the magnitude of $L_z(t)$ and its sign (i.e., the phase in the oscillation of angular momentum) evidently depend on the type of excitation. In Figure 5a, π electrons start to rotate clockwise (counterclockwise) for $\mathbf{e}_{\mathrm{in}}$ ($\mathbf{e}_{\mathrm{out}}$) excitation, while the amplitude of $L_z(t)$ reaches its maximum at $t = 5.4$ fs in both cases. This agrees with the difference in the initial relative phase θ by π between the two linear polarization vectors predicted in the model analysis. Compared to $\mathbf{e}_{\mathrm{in}}$ and $\mathbf{e}_{\mathrm{out}}$ excitations, the magnitudes of $L_z(t)$ for circular polarizations in Figure 5b grow earlier. In addition, the largest amplitude of angular momentum for $\mathbf{e}_{+1}$ ($\mathbf{e}_{-1}$) excitation appears 1–2 fs later (earlier) than those in Figure 5a. The curves of $L_z(t)$ in Figure 5b, which oscillate with different phases from those for linear polarizations, are fairly consistent with $\theta = \pm(\chi_{\mathrm{H}} - \chi_{\mathrm{L}}) = \pm 0.35\pi$ for $\mathbf{e}_{\pm1}$. These agreements with the model analysis manifest the controllability of the initial
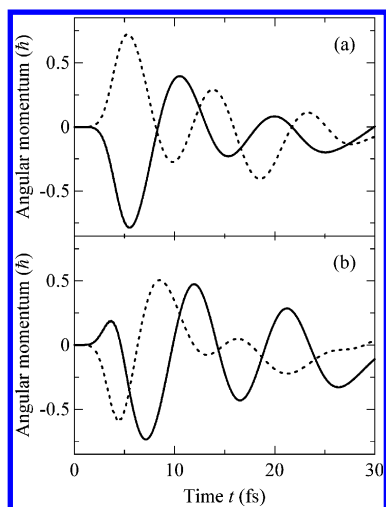
Figure 5. Expectation value of the electronic angular momentum $L_z(t)$ in DCP irradiated by (a) linearly and (b) circularly polarized UV laser pulses. In panel a, the solid and dotted lines denote the expectation values for $\mathbf{e}_{in}$ and $\mathbf{e}_{out}$ excitations, respectively; in panel b, the solid and dotted lines denote those for $\mathbf{e}_{+1}$ and $\mathbf{e}_{-1}$ excitations, respectively. The laser pulses fully decay at $t = 7.26$ fs.
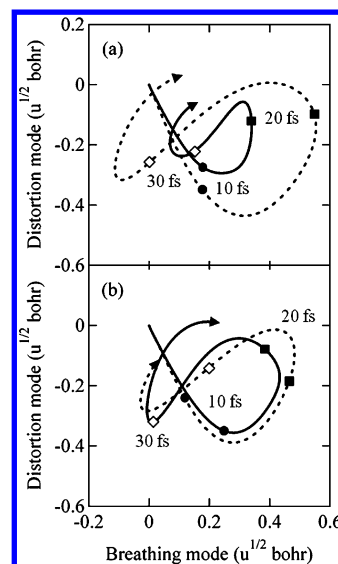

Figure 6. Expectation value of the normal coordinates $\mathbf{Q}(t)$ of the breathing and distortion modes in DCP irradiated by (a) linearly and (b) circularly polarized UV laser pulses. In panel a, the solid and dotted lines denote the expectation values for $\mathbf{e}_{in}$ and $\mathbf{e}_{out}$ excitations, respectively; in panel b, the solid and dotted lines denote those for $\mathbf{e}_{+1}$ and $\mathbf{e}_{-1}$ excitations, respectively. The laser pulses fully decay at $t = 7.26$ fs. The values of $\mathbf{Q}(t)$ are plotted up to $t = 40$ fs.

relative phase of the superposed quasi-degenerate states by laser polarization. As in eqs 36 and 40, the magnitude of $L_z(t)$ turns to decrease or even the rotation direction of π electrons flips before $t = t_d = 7.26$ fs and after irradiation the angular momentum oscillates with the period of $T = \pi/\Delta\omega = 9.4$ fs as shown in Figure 5. A little difference in the oscillation period between the four types of excitations stems from the fact that the energy gap between the two adiabatic PESs in the regions where the WPs run depends on the type of excitation. Nevertheless, the amplitude of its oscillation is gradually reduced for both linear and circular polarizations, which is a characteristic feature absent in a frozen-nuclei model. As we pointed out in ref 41, the reduction in the angular momentum is attributed to two factors: decrease of the overlap between the WPs moving on the relevant two adiabatic PESs, which is observed even within the Born–Oppenheimer approximation (BOA),[58] and electronic relaxation due to nonadiabatic couplings shown in Figure 4, which is the major factor. Both of the factors cause the loss of a superposition of $|L\rangle$ and $|H\rangle$. The oscillatory curves of $L_z(t)$ for $\mathbf{e}_{in}$ and $\mathbf{e}_{+1}$ excitations can be approximately expressed by a sinusoidal exponential decay. The lifetime of the decay is ~6 fs for $\mathbf{e}_{in}$ and ~18 fs for $\mathbf{e}_{+1}$, of which difference originates from the different rates of nonadiabatic transition in Figure 4a,c. On the other hand, the amplitudes of $L_z(t)$ for $\mathbf{e}_{out}$ and $\mathbf{e}_{-1}$ excitations do not undergo a monotonic decrease but make a small transient recovery (around $t \sim 14$–20 fs for $\mathbf{e}_{out}$ and $t \sim 18$–24 fs for $\mathbf{e}_{-1}$). This recovery arises from the regeneration of the superposition of $|L\rangle$ and $|H\rangle$ due to the upward population transfer in the respective time ranges in Figure 4b,d. The results in Figure 5 confirm that π-electron rotation can be controlled by the polarization of a laser pulse, although it is attenuated on the time scale of several tens of femtoseconds by nonadiabatic couplings.

Figure 6 depicts the expectation value of the normal coordinates $\mathbf{Q}(t) \equiv \langle\Psi(t)|\hat{\mathbf{Q}}|\Psi(t)\rangle$, with $\hat{\mathbf{Q}}$ being the operator of $\mathbf{Q}$. In Figure 6a, the behaviors of $\mathbf{Q}(t)$ triggered by linearly polarized laser pulses are remarkably dependent on the polarization direction: The vibrational amplitude for $\mathbf{e}_{out}$ excitation is more than two-times larger than that for $\mathbf{e}_{in}$

excitation. Contrary to this, in Figure 6b, the vibration of DCP differs only slightly between circular polarizations and the trajectories of $\mathbf{Q}(t)$ are located between those for linear ones. These findings are reinforced by vibrational spectral analysis. The frequency spectrum of the WP on the lower PES, $\psi_L(\mathbf{Q},t)$, after the nonadiabatic transition from $|H\rangle$ to $|L\rangle$ is given by the Fourier transform of its autocorrelation function:[59]

$$\sigma_L(\omega) \equiv Re \int_{t_i}^{t_f} dt\ e^{(i\omega - 1/\tau)(t-t_i)} \int d\mathbf{Q}\ \psi_L^*(\mathbf{Q},t_i)\ \psi_L(\mathbf{Q},t)$$

(42)

The parameter τ was introduced to smooth the spectra and set at 39.6 fs, which is longer than the vibrational periods of the breathing and distortion modes (28.8 and 21.2 fs). The values of t_i for $\mathbf{e}_{in}$, $\mathbf{e}_{out}$, $\mathbf{e}_{+1}$, and $\mathbf{e}_{-1}$ excitations were 14.0, 10.0, 34.0, and 13.0 fs, respectively, and $t_f - t_i = 99.1$ fs for all of them. The zero of ω was chosen to be the minimum of the relevant PES. The frequency spectra for the four types of excitations are displayed in Figure 7. For $\mathbf{e}_{in}$ excitation, the maximum value of $\sigma_L(\omega)$ is located at $\tilde{\nu} \sim 1400$ cm^{-1} and another peak appears at $\tilde{\nu} \sim 2500$ cm^{-1} in Figure 7a; for $\mathbf{e}_{out}$ excitation, the strongest peak of $\sigma_L(\omega)$ is found at $\tilde{\nu} \sim 2500$ cm^{-1} and besides a couple of strong peaks are identified at $\tilde{\nu} > 3000$ cm^{-1}. The wave numbers of 1400, 2500, and 3000 cm^{-1} are almost identical to those of the lowest three vibrational states of $|G\rangle$ owing to the analogy between $|G\rangle$ and $|L\rangle$ in the PES around its minimum. The frequency spectra for linear polarizations in Figure 7a support that at $t > t_i$ $\psi_L(\mathbf{Q},t)$ is mainly composed of low (high) vibrational quantum states for $\mathbf{e}_{in}$ ($\mathbf{e}_{out}$) excitation. In marked distinction from linear polarizations, the spectral features for circular ones in Figure 7b are quite similar: The primary peaks of $\sigma_L(\omega)$ for $\mathbf{e}_{+1}$ and $\mathbf{e}_{-1}$ excitations are both at $\tilde{\nu} \sim 1400$ cm^{-1}, whereas the intensities of the other peaks are a little stronger for the latter. This obviously indicates that $\psi_L(\mathbf{Q},t)$ contains the same frequency components for left and right circular polarizations after the nonadiabatic transition.
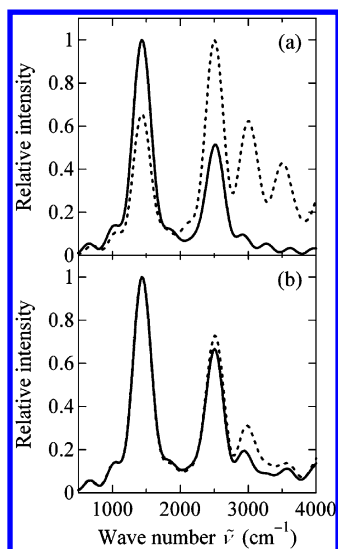
Figure 7. Frequency spectra of $\psi_L(\mathbf{Q},t)$, $\sigma_L(\omega)$, defined by eq 42 for DCP irradiated by (a) linearly and (b) circularly polarized UV laser pulses. In panel a, the solid and dotted lines denote the spectra for $\mathbf{e}_{in}$ and $\mathbf{e}_{out}$ excitations, respectively; in panel b, the solid and dotted lines denote those for $\mathbf{e}_{+1}$ and $\mathbf{e}_{-1}$ excitations, respectively. In each case, the values of $\sigma_L(\omega)$ were scaled so that the maximum value is unity.

3.4. Comparison to the Born–Oppenheimer Approximation.

We also carried out nuclear WP simulations within the BOA, in which the nonadiabatic coupling between the quasi-degenerate states was completely neglected and thereby the WPs simply propagated on the individual PESs. As seen in Figure 8, the laser-polarization dependence of the phase in the oscillation of angular momentum is observed in this case as well; however, other features in Figures 5 and 6 that are deemed to be caused by nonadiabatic couplings disappear under the BOA as expected. The amplitude of $L_z(t)$ does not decay exponentially but exhibits periodic reduction and
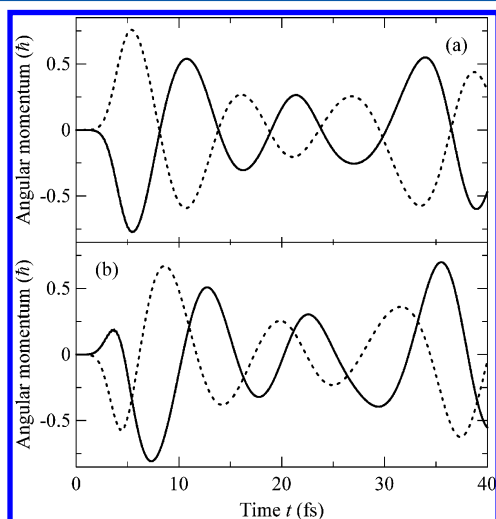

Figure 8. Expectation value of the electronic angular momentum $L_z(t)$ in DCP irradiated by (a) linearly and (b) circularly polarized UV laser pulses under the BOA. In panel a, the solid and dotted lines denote the expectation values for $\mathbf{e}_{in}$ and $\mathbf{e}_{out}$ excitations, respectively; in panel b, the solid and dotted lines denote those for $\mathbf{e}_{+1}$ and $\mathbf{e}_{-1}$ excitations, respectively. The laser pulses fully decay at $t = 7.26$ fs. The values of $L_z(t)$ are plotted up to $t = 40$ fs.

recovery in turn owing to the temporal change in the WP overlap. The trajectory of $\mathbf{Q}(t)$ in Figure 9 hardly depends on
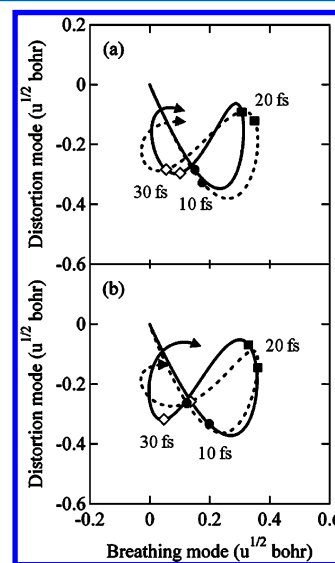

Figure 9. Expectation value of the normal coordinates $\mathbf{Q}(t)$ of the breathing and distortion modes in DCP irradiated by (a) linearly and (b) circularly polarized UV laser pulses under the BOA. In panel a, the solid and dotted lines denote the expectation values for $\mathbf{e}_{in}$ and $\mathbf{e}_{out}$ excitations, respectively; in panel b, the solid and dotted lines denote those for $\mathbf{e}_{+1}$ and $\mathbf{e}_{-1}$ excitations, respectively. The laser pulses fully decay at $t = 7.26$ fs. The values of $\mathbf{Q}(t)$ are plotted up to $t = 40$ fs.

the type of excitation and the vibrational amplitude is larger than that for $\mathbf{e}_{in}$ excitation in Figure 6a but smaller than those for circular polarizations in Figure 6b. These facts corroborate that the laser-polarization effects on nonadiabatic transition indeed give birth to the polarization-dependent behaviors in π-electron rotation and molecular vibration such as the decay of angular momentum with different lifetimes.

3.5. Laser Control of Interference between Nuclear Wave Packets.

To take a close look at the laser-polarization effects on nonadiabatic transition, the propagations of the WPs on the relevant two adiabatic PESs are illustrated in Figure 10. For both linear and circular polarizations, the probability densities $|\psi_L(\mathbf{Q},t)|^2$ and $|\psi_H(\mathbf{Q},t)|^2$ created in the two excited states at $t \sim 5$ fs resemble that of the initial WP $|\psi_G(\mathbf{Q},0)|^2$, and then the WPs start to move along the gradient of each PES. Yet, the nonadiabatic nature of vibronic dynamics in this system emerges differently for the four types of excitations when the WPs approach the avoided crossing. For $\mathbf{e}_{in}$ excitation, the WP on the higher PES is diminished by nonadiabatic transition at $t \sim 12$ fs and the contour map of $|\psi_L(\mathbf{Q},t)|^2$ in Figure 10a clearly displays the node originating from the interference; thereafter, the WPs on the two adiabatic PESs are deformed largely. In contrast, the WPs for $\mathbf{e}_{out}$ excitation in Figure 10b maintain a Gaussian-like form even after the nonadiabatic transition, which is already in progress at $t \sim 8$ fs. The WPs excited by circularly polarized laser pulses behave as expected from the tendencies of the populations in Figure 4c,d. In Figure 10c, only a small fraction of $\psi_H(\mathbf{Q},t)$ has been transferred to $|L\rangle$ until $t \sim 12$ fs and no interference patterns are found in the WPs for $\mathbf{e}_{+1}$ excitation. The WPs for $\mathbf{e}_{-1}$ excitation in Figure 10d have intermediate features between those for $\mathbf{e}_{in}$ and $\mathbf{e}_{out}$ excitations: They do not exhibit a clear interference but the shape of $|\psi_L(\mathbf{Q},t)|^2$ is distorted from a Gaussian especially at $t \sim 12$ fs. As
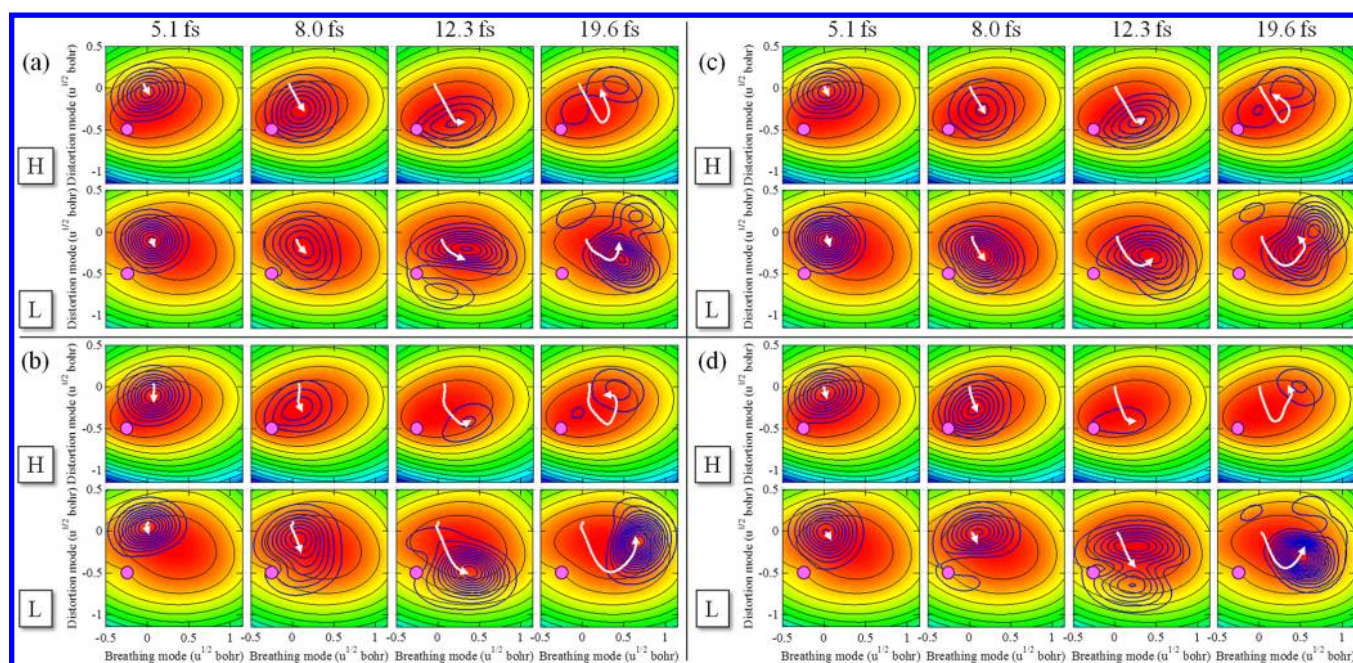
Figure 10. Propagation of the adiabatic WPs on the two-dimensional adiabatic PESs of $|L\rangle$ and $|H\rangle$ for (a) $\mathbf{e}_{in}$, (b) $\mathbf{e}_{out}$, (c) $\mathbf{e}_{+1}$, and (d) $\mathbf{e}_{-1}$ excitations. The origin of the PESs is the optimized geometry of $|G\rangle$ and the avoided crossing is designated by a circle. The bold contours represent the probability densities $|\psi_L(\mathbf{Q},t)|^2$ and $|\psi_H(\mathbf{Q},t)|^2$. The arrows indicate the motion of the center of the WPs.

a consequence of nonadiabatic couplings, the center of $\psi_L(\mathbf{Q},t)$, which contributes dominantly to $\mathbf{Q}(t)$ in Figure 6, proceeds in a low-energy (high-energy) region on the lower PES for $\mathbf{e}_{in}$ ($\mathbf{e}_{out}$) excitation, whereas the motions of the center for circular polarizations are analogous to each other.

The laser-polarization effects on the populations, expectation values $L_z(t)$ and $\mathbf{Q}(t)$, and WPs can be understood in terms of interferences between the WP existing on the original PES and that created by nonadiabatic couplings. As mentioned in the model analysis in section 2.2, a linearly polarized laser pulse with $\mathbf{e}_{out}$ achieves $\theta = \pi$; in other words, it initially produces a linear combination of $\psi_L(\mathbf{Q},t)$ and $\psi_H(\mathbf{Q},t)$ out of phase. Then, their relative quantum phase evolves during irradiation [by $-\vartheta(t)$ in the cases of rectangular-envelope pulses] and also gains a dynamical phase associated with potential shape as the WPs move on each PES. In nonadiabatic transition, an additional phase shift is further imposed on the WP created by nonadiabatic couplings, which interferes with that on the other PES. We do not quantify the additional phase, but the downward population transfer around $t \sim 5 - 10$ fs in Figure 4b implies opposite interferences on the two PESs: The WPs are almost in phase and interfere constructively on the lower PES, whereas those on the higher one are out of phase with destructive interference. The constructive interference works particularly on high vibrational quantum states in $\psi_L(\mathbf{Q},t)$. The direction of the population transfer flips as the relative quantum phase develops. For $\mathbf{e}_{in}$ excitation in which the two excited WPs are in phase ($\theta = 0$), the interference effects are reversed from those for $\mathbf{e}_{out}$ excitation: The interference is destructive on the lower PES but constructive on the higher one around $t \sim 5-10$ fs. The resultant upward population transfer is small because the amount of the WP created by the nonadiabatic transition from $|L\rangle$ to $|H\rangle$ is less than that for the transition from $|H\rangle$ to $|L\rangle$. The WPs on the two PESs then reach the avoided crossing and the reverse population transfer takes place around $t \sim 10-14$ fs. The interference enhances low vibrational quantum states

in $\psi_L(\mathbf{Q},t)$, increasing the probability density in a low-energy region on the lower PES as seen in Figure 10a. In the cases of circular polarizations, $\psi_L(\mathbf{Q},t)$ and $\psi_H(\mathbf{Q},t)$ are initially neither in phase nor out of phase because $\theta = \pm 0.35\pi$ for $\mathbf{e}_{\pm 1}$. Hence, no fully constructive or destructive interference occurs on either PES at $t \sim 5 - 10$ fs, resulting in the vibrational amplitudes in Figure 6b that are intermediate between those for linear polarizations in Figure 6a. As the relative quantum phase between the WPs evolves in the negative direction, for $\mathbf{e}_{-1}$ excitation with $\theta = -0.35\pi$, the downward population transfer, which requires constructive and destructive interferences on the lower and higher PESs, respectively, appears at $t \sim 8-13$ fs; for $\mathbf{e}_{+1}$ excitation with $\theta = 0.35\pi$, the WPs pass through the avoided crossing before matching the requirement of interference for population transfer and thus the nonadiabatic transition is unfinished until they come closer again to the avoided crossing at $t \sim 30$ fs.

The nuclear WP simulations demonstrated that the initial relative phase θ between the WPs of the quasi-degenerate excited states, which is determined by the ellipticity angle β and orientation angle δ of the incident light, governs not only π-electron rotation but also the subsequent molecular vibration through nonadiabatic couplings. What is more, we can also manipulate the time-dependent phase due to irradiation, namely, $\vartheta(t)$ by tuning the other laser parameters such as the peak field strength ε_p and pulse duration t_d. This suggests that in principle it is possible to produce a superposition of the quasi-degenerate states with an arbitrary relative phase after excitation by a laser pulse of arbitrary polarization. Ultimately, the interference between nuclear WPs in nonadiabatic transition can be controlled as desired by means of ultrashort laser pulses, leading to sophisticated control of molecular vibrations.

4. CONCLUSIONS

We have theoretically investigated the nonadiabatically coupled vibronic dynamics of aromatic molecules with quasi-degenerate π-electronic states excited by an ultrashort UV laser pulse of arbitrary polarization. First, the concept of electronic angular momentum eigenstates in aromatic molecules was introduced to quantify laser-driven π-electron rotation (ring current) in reference to MO theory. Next, for the purpose of analyzing the role of laser polarization in the optical excitation process, we employed the V-type three-level model under the frozen-nuclei condition and derived general formulations of the coherent electronic WP and angular-momentum expectation value in both degenerate and quasi-degenerate systems. The initial relative phase between the quasi-degenerate excited states, θ, is determined by the ellipticity angle β and orientation angle δ of an applied laser field, and the relation among the three variables was provided in eq 18. The time-dependent part of the relative quantum phase, $\vartheta(t)$, is adjustable by the laser pulse as well. It is therefore possible to create a desired superposition of the quasi-degenerate states by applying ultrashort laser pulses. The angular-momentum expectation value follows the temporal behavior in the relative quantum phase as shown in eq 36 and oscillates after irradiation with the period corresponding to the energy gap between the quasi-degenerate states.

Nuclear WP simulations were also carried out with a model system of DCP and the numerical results confirmed the controllability of the phase in the oscillation of angular momentum. The angular momentum of π electrons, however, decays on the time scale of several tens of femtoseconds by nonadiabatic couplings. The comparison in the expectation values of vibrational coordinates between the linear and circular polarization cases revealed an interesting finding: The amplitude of the molecular vibration coupled to π-electron rotation is prominently dependent on the orientation of linear polarization vectors rather than the helicity of circular polarization. This characteristic dependence of vibrational amplitudes on laser polarization is ascribed to the interference effects in nonadiabatic transition dictated by the relative quantum phase between the WPs. The results in this paper suggest the potential application of attosecond/several-femtosecond polarized laser pulses as a promising tool to control molecular vibrations through the WP interference in non-adiabatic transition.

We expect that the knowledge obtained for aromatic molecules serves as a basis for studying more complicated polarization-dependent dynamics in larger systems, e.g., intense-field fragmentation of C_{60}.[28] Control of nonadiabatic vibrational/fragmentation dynamics induced by multiphoton electronic excitation is a worthwhile subject for future research.

AUTHOR INFORMATION

Corresponding Author

*E-mail: fujimurayuichi@m.tohoku.ac.jp.

Notes

The authors declare no competing financial interest.

ACKNOWLEDGMENTS

REFERENCES

(1) (a) Arasaki, Y.; Takatsuka, K.; Wang, K.; McKoy, V. *J. Chem. Phys.* **2010**, *132*, 124307. (b) Arasaki, Y.; Wang, K.; McKoy, V.; Takatsuka, K. *Phys. Chem. Chem. Phys.* **2011**, *13*, 8681.

(2) (a) Bisgaard, C. Z.; Clarkin, O. J.; Wu, G.; Lee, A. M. D.; Geßner, O.; Hayden, C. C.; Stolow, A. *Science* **2009**, *323*, 1464. (b) Hockett, P.; Bisgaard, C. Z.; Clarkin, O. J.; Stolow, A. *Nat. Phys.* **2011**, *7*, 612.

(3) (a) Suzuki, Y.; Stener, M.; Seideman, T. *Phys. Rev. Lett.* **2002**, *89*, 233002. (b) Suzuki, Y.; Stener, M.; Seideman, T. *J. Chem. Phys.* **2003**, *118*, 4432.

(4) (a) Horio, T.; Fujii, T.; Suzuki, Y.; Suzuki, T. *J. Am. Chem. Soc.* **2009**, *131*, 10392. (b) Liu, S. Y.; Ogi, Y.; Fuji, T.; Nishizawa, K.; Horio, T.; Mizuno, T.; Kohguchi, H.; Nagasono, M.; Togashi, T.; Tono, K.; et al. *Phys. Rev. A* **2010**, *81*, 031403(R).

(5) Fujii, T.; Suzuki, Y.; Horio, T.; Suzuki, T.; Mitrić, R.; Werner, U.; Bonačić-Koutecký, V. *J. Chem. Phys.* **2010**, *133*, 234303.

(6) Abulimiti, B.; Zhu, R.; Long, J.; Xu, Y.; Liu, Y.; Ghazal, A. Y.; Yang, M.; Zhang, B. *J. Chem. Phys.* **2011**, *134*, 234301.

(7) Dion, C. M.; Bandrauk, A. D.; Atabek, O.; Keller, A.; Umeda, H.; Fujimura, Y. *Chem. Phys. Lett.* **1999**, *302*, 215.

(8) (a) Sakai, H.; Safvan, C. P.; Larsen, J. J.; Hilligsøe, K. M.; Hald, K.; Stapelfeldt, H. *J. Chem. Phys.* **1999**, *110*, 10235. (b) Larsen, J. J.; Sakai, H.; Safvan, C. P.; Wendt-Larsen, I.; Stapelfeldt, H. *J. Chem. Phys.* **1999**, *111*, 7774.

(9) Larsen, J. J.; Hald, K.; Bjerre, N.; Stapelfeldt, H.; Seideman, T. *Phys. Rev. Lett.* **2000**, *85*, 2470.

(10) Hoki, K.; Fujimura, Y. *Chem. Phys.* **2001**, *267*, 187.

(11) Stapelfeldt, H.; Seideman, T. *Rev. Mod. Phys.* **2003**, *75*, 543.

(12) (a) Nakagami, K.; Mizumoto, Y.; Ohtsuki, Y. *J. Chem. Phys.* **2008**, *129*, 194103. (b) Abe, H.; Ohtsuki, Y. *Phys. Rev. A* **2011**, *83*, 053410.

(13) (a) Sakai, H.; Minemoto, S.; Nanjo, H.; Tanji, H.; Suzuki, T. *Phys. Rev. Lett.* **2003**, *90*, 083001. (b) Minemoto, S.; Nanjo, H.; Tanji, H.; Suzuki, T.; Sakai, H. *J. Chem. Phys.* **2003**, *118*, 4052.

(14) Tanji, H.; Minemoto, S.; Sakai, H. *Phys. Rev. A* **2005**, *72*, 063401.

(15) Takemoto, N.; Yamanouchi, K. *Chem. Phys. Lett.* **2008**, *451*, 1.

(16) Seideman, T. *Phys. Rev. Lett.* **1999**, *83*, 4971.

(17) (a) Rosca-Pruna, F.; Vrakking, M. J. J. *Phys. Rev. Lett.* **2001**, *87*, 153902;(b) Rosca-Pruna, F.; Vrakking, M. J. J. *J. Chem. Phys.* **2002**, *116*, 6567;(c) Rosca-Pruna, F.; Vrakking, M. J. J. *J. Chem. Phys.* **2002**, *116*, 6579.

(18) Renard, V.; Renard, M.; Guérin, S.; Pashayan, Y. T.; Lavorel, B.; Faucher, O.; Jauslin, H. R. *Phys. Rev. Lett.* **2003**, *90*, 153601.

(19) Dooley, P. W.; Litvinyuk, I. V.; Lee, K. F.; Rayner, D. M.; Spanner, M.; Villeneuve, D. M.; Corkum, P. B. *Phys. Rev. A* **2003**, *68*, 023406.

(20) (a) Péronne, E.; Poulsen, M. D.; Bisgaard, C. Z.; Stapelfeldt, H. *Phys. Rev. Lett.* **2003**, *91*, 043003. (b) Bisgaard, C. Z.; Poulsen, M. D.; Péronne, E.; Stapelfeldt, H. *Phys. Rev. Lett.* **2004**, *92*, 173004. (c) Poulsen, M. D.; Péronne, E.; Stapelfeldt, H.; Bisgaard, C. Z.; Viftrup, S. S.; Hamilton, E.; Seideman, T. *J. Chem. Phys.* **2004**, *121*, 783. (d) Péronne, E.; Poulsen, M. D.; Stapelfeldt, H.; Bisgaard, C. Z.; Hamilton, E.; Seideman, T. *Phys. Rev. A* **2004**, *70*, 063410.

(21) Hamilton, E.; Seideman, T.; Ejdrup, T.; Poulsen, M. D.; Bisgaard, C. Z.; Viftrup, S. S.; Stapelfeldt, H. *Phys. Rev. A* **2005**, *72*, 043402.

(22) Kanai, T.; Minemoto, S.; Sakai, H. *Nature* **2005**, *435*, 470.

(23) Boutu, W.; Haessler, S.; Merdji, H.; Breger, P.; Waters, G.; Stankiewicz, M.; Frasinski, L. J.; Taieb, R.; Caillat, J.; Maquet, A.; et al. *Nat. Phys.* **2008**, *4*, 545.

(24) McFarland, B. K.; Farrell, J. P.; Bucksbaum, P. H.; Gühr, M. *Science* **2008**, *322*, 1232.

(25) Itatani, J.; Levesque, J.; Zeidler, D.; Niikura, H.; Pépin, H.; Kieffer, J. C.; Corkum, P. B.; Villeneuve, D. M. *Nature* **2004**, *432*, 867.

(26) Haessler, S.; Caillat, J.; Boutu, W.; Giovanetti-Teixeira, C.; Ruchon, T.; Auguste, T.; Diveki, Z.; Breger, P.; Maquet, A.; Carré, B.; et al. *Nat. Phys.* **2010**, *6*, 200.

11271

dx.doi.org/10.1021/jp305284w | *J. Phys. Chem. A* 2012, 116, 11260–11272

(27) Vozzi, C.; Negro, M.; Calegari, F.; Sansone, G.; Nisoli, M.; De Silvestri, S.; Stagira, S. *Nat. Phys.* **2011**, *7*, 822.

(28) (a) Hertel, I. V.; Shchatsinin, I.; Laarmann, T.; Zhavoronkov, N.; Ritze, H.-H.; Schulz, C. P. *Phys. Rev. Lett.* **2009**, *102*, 023003. (b) Shchatsinin, I.; Ritze, H.-H.; Schulz, C. P.; Hertel, I. V. *Phys. Rev. A* **2009**, *79*, 053414.

(29) (a) Barth, I.; Manz, J. *Angew. Chem.* **2006**, *118*, 3028;(b) Barth, I.; Manz, J. *Angew. Chem., Int. Ed.* **2006**, *45*, 2962. (c) Barth, I.; Manz, J.; Shigeta, Y.; Yagi, K. *J. Am. Chem. Soc.* **2006**, *128*, 7043. (d) Barth, I.; Manz, J. In *Progress in Ultrafast Intense Laser Science*; Yamanouchi, K., Gerber, G., Bandrauk, A. D., Eds.; Springer: Berlin, 2010; Vol. *6*, pp 21−44.

(30) Barth, I.; Manz, J.; Sebald, P. *Chem. Phys.* **2008**, *346*, 89.

(31) Barth, I.; Manz, J.; Serrano-Andrés, L. *Chem. Phys.* **2008**, *347*, 263.

(32) (a) Barth, I.; Serrano-Andrés, L.; Seideman, T. *J. Chem. Phys.* **2008**, *129*, 164303;(b) Barth, I.; Serrano-Andrés, L.; Seideman, T. *J. Chem. Phys.* **2009**, *130*, 109901.

(33) Yonehara, T.; Takatsuka, K. *Chem. Phys.* **2009**, *366*, 115.

(34) Takatsuka, K.; Yonehara, T. *Phys. Chem. Chem. Phys.* **2011**, *13*, 4987.

(35) (a) Alon, O. E.; Averbukh, V.; Moiseyev, N. *Phys. Rev. Lett.* **1998**, *80*, 3743. (b) Baer, R.; Neuhauser, D.; Ždánská, P. R.; Moiseyev, N. *Phys. Rev. A* **2003**, *68*, 043406.

(36) (a) Ceccherini, F.; Bauer, D. *Phys. Rev. A* **2001**, *64*, 033423. (b) Ceccherini, F.; Bauer, D.; Cornolti, F. *J. Phys. B* **2001**, *34*, 5017.

(37) Nobusada, K.; Yabana, K. *Phys. Rev. A* **2007**, *75*, 032518.

(38) Ulusoy, I. S.; Nest, M. *J. Am. Chem. Soc.* **2011**, *133*, 20230.

(39) (a) Kanno, M.; Kono, H.; Fujimura, Y. *Angew. Chem.* **2006**, *118*, 8163;(b) Kanno, M.; Kono, H.; Fujimura, Y. *Angew. Chem., Int. Ed.* **2006**, *45*, 7995.

(40) Kanno, M.; Hoki, K.; Kono, H.; Fujimura, Y. *J. Chem. Phys.* **2007**, *127*, 204314.

(41) Kanno, M.; Kono, H.; Fujimura, Y.; Lin, S. H. *Phys. Rev. Lett.* **2010**, *104*, 108302.

(42) Kanno, M.; Kono, H.; Fujimura, Y. In *Progress in Ultrafast Intense Laser Science*; Yamanouchi, K., Charalambidis, D., Normand, D., Eds.; Springer: Berlin, 2011; Vol. *7*, pp 53−78.

(43) Mineo, H.; Kanno, M.; Kono, H.; Chao, S. D.; Lin, S. H.; Fujimura, Y. *Chem. Phys.* **2012**, *392*, 136.

(44) Salem, L. *The Molecular Orbital Theory of Conjugated Systems*; Benjamin: New York, 1966; pp 112−116.

(45) Frost, A. A.; Musulin, B. *J. Chem. Phys.* **1953**, *21*, 572.

(46) Rubio, M.; Ross, B. O.; Serrano-Andrés, L.; Merchán, M. *J. Chem. Phys.* **1999**, *110*, 7202.

(47) Sundholm, D. *Chem. Phys. Lett.* **2000**, *317*, 392.

(48) (a) Shore, B. W. *The Theory of Coherent Atomic Excitation*; Wiley: New York, 1990; Vol. *2*, pp 778−787. (b) Vol. *1*, pp 235−239. (c) Vol. *1*, pp 304−309.

(49) (a) Selle, R.; Nuernberger, P.; Langhojer, F.; Dimler, F.; Fechner, S.; Gerber, G.; Brixner, T. *Opt. Lett.* **2008**, *33*, 803. (b) Nuernberger, P.; Selle, R.; Langhojer, F.; Dimler, F.; Fechner, S.; Gerber, G.; Brixner, T. *J. Opt. A* **2009**, *11*, 085202.

(50) (a) Seidel, M. T.; Zhang, Z.; Yan, S.; Tan, H.-S. *J. Opt. Soc. Am. B* **2011**, *28*, 1146. (b) Seidel, M. T.; Zhang, Z.; Yan, S.; Wells, K. L.; Tan, H.-S. *J. Opt. Soc. Am. B* **2011**, *28*, 2718.

(51) Baer, M. *Beyond Born-Oppenheimer*; Wiley: Hoboken, NJ, 2006; pp 26−57.

(52) Sarkar, B.; Adhikari, S. *Int. J. Quantum Chem.* **2009**, *109*, 650.

(53) Simah, D.; Hartke, B.; Werner, H.-J. *J. Chem. Phys.* **1999**, *111*, 4523.

(54) Werner, H.-J.; Knowles, P. J.; Lindh, R.; Manby, F. R.; Schütz, M.; Celani, P.; Korona, T.; Rauhut, G.; Amos, R. D.; Bernhardsson, A.; et al. *MOLPRO*, version 2006.1; Cardiff, U.K., 2006.

(55) Ohtsuki, Y.; Nakagami, K.; Fujimura, Y. In *Advances in Multi-Photon Processes and Spectroscopy*; Lin, S. H., Villaeys, A. A., Fujimura, Y., Eds.; World Scientific: Singapore, 2001; Vol. *13*, pp 1−127.

(56) Gross, P.; Neuhauser, D.; Rabitz, H. *J. Chem. Phys.* **1992**, *96*, 2834.

(57) Levine, I. N. *Quantum Chemistry*, 6th ed.; Prentice Hall: Hoboken, NJ, 2009; pp 471−635.

(58) Born, M.; Oppenheimer, J. R. *Ann. Phys.* **1927**, *84*, 457.

(59) Tannor, D. J. *Introduction to Quantum Mechanics: A Time-Dependent Perspective*; University Science Books: Sausolito, CA, 2007; pp 81−86.